REPORT DOCUMENTATION PAGE

Form Approved
OMB No. 0704-0188

PLEASE DO NOT RETURN YOUR FORM TO THE ABOVE ADDRESS.

1. REPORT DATE *(DD-MM-YYYY)*	2. REPORT TYPE	3. DATES COVERED *(From - To)*
22-12-2022	Final Technical Report	19-05-2021 - 18-05-2022

4. TITLE AND SUBTITLE
Epitaxial Growth and Characterization of Topological a-Sn and a-Sn1-xGex Films

5a. CONTRACT NUMBER
W911NF-21-2-0140

5b. GRANT NUMBER

5c. PROGRAM ELEMENT NUMBER

6. AUTHOR(S)
Palmstrom, Christopher J.

5d. PROJECT NUMBER
0011629554

5e. TASK NUMBER

5f. WORK UNIT NUMBER

7. PERFORMING ORGANIZATION NAME(S) AND ADDRESS(ES)
UNIVERSITY OF CALIFORNIA, SANTA BARBARA
OFFICE OF RESEARCH
3227 CHEADLE HALL
SANTA BARBARA CA 93106-0001

8. PERFORMING ORGANIZATION REPORT NUMBER

9. SPONSORING/MONITORING AGENCY NAME(S) AND ADDRESS(ES)
US ARMY ACC-APG-RTP W911NF
800 PARK OFFICE DRIVE
SUITE 4229
RESEARCH TRIANGLE PARK NC 27709

10. SPONSOR/MONITOR'S ACRONYM(S)

11. SPONSOR/MONITOR'S REPORT NUMBER(S)

12. DISTRIBUTION/AVAILABILITY STATEMENT
Approved for Public Release; Distribution in Unlimited

13. SUPPLEMENTARY NOTES

14. ABSTRACT

Epitaxial single crystal films of alpha-tin and alpha-tin alloyed with germanium have been grown using molecular beam epitaxy on indium antimonide surfaces. By alloying with germanium, the strain in films could be controlled from compressive to tensile. The resulting electronic structure of the films was studied using angle-resolved photoelectron spectroscopy, scanning tunneling microscopy and spectroscopy without exposure to air, and cryogenic temperature magnetotransport. Preliminary results confirm that thin films of alpha-tin alloyed with germanium are topological insulators. Further, tensile strain does not appear to open an energy gap in the alpha-Sn surface states intrinsically, but the gap is actually a result of either band occupation or lattice distortion. It was also found that alpha-tin growth on antimony-terminated indium antimonide surfaces decreased indium segregation and thus widened the growth window.

15. SUBJECT TERMS
Alpha-tin, molecular beam epitaxy, angle-resolved photoelectron spectroscopy, electronic band structure, topological insulator

16. SECURITY CLASSIFICATION OF:			17. LIMITATION OF ABSTRACT	18. NUMBER OF PAGES	19a. NAME OF RESPONSIBLE PERSON
a. REPORT	b. ABSTRACT	c. THIS PAGE			Christopher J. Palmstrom
UU	SAR	SAR	SAR	17	19b. TELEPHONE NUMBER *(Include area code)* 805-893-3618

Reset

INSTRUCTIONS FOR COMPLETING SF 298

1. REPORT DATE. Full publication date, including day, month, if available. Must cite at least the year and be Year 2000 compliant, e.g. 30-06-1998; xx-06-1998; xx-xx-1998.

2. REPORT TYPE. State the type of report, such as final, technical, interim, memorandum, master's thesis, progress, quarterly, research, special, group study, etc.

3. DATES COVERED. Indicate the time during which the work was performed and the report was written, e.g., Jun 1997 - Jun 1998; 1-10 Jun 1996; May - Nov 1998; Nov 1998.

4. TITLE. Enter title and subtitle with volume number and part number, if applicable. On classified documents, enter the title classification in parentheses.

5a. CONTRACT NUMBER. Enter all contract numbers as they appear in the report, e.g. F33615-86-C-5169.

5b. GRANT NUMBER. Enter all grant numbers as they appear in the report, e.g. AFOSR-82-1234.

5c. PROGRAM ELEMENT NUMBER. Enter all program element numbers as they appear in the report, e.g. 61101A.

5d. PROJECT NUMBER. Enter all project numbers as they appear in the report, e.g. 1F665702D1257; ILIR.

5e. TASK NUMBER. Enter all task numbers as they appear in the report, e.g. 05; RF0330201; T4112.

5f. WORK UNIT NUMBER. Enter all work unit numbers as they appear in the report, e.g. 001; AFAPL30480105.

6. AUTHOR(S). Enter name(s) of person(s) responsible for writing the report, performing the research, or credited with the content of the report. The form of entry is the last name, first name, middle initial, and additional qualifiers separated by commas, e.g. Smith, Richard, J, Jr.

7. PERFORMING ORGANIZATION NAME(S) AND ADDRESS(ES). Self-explanatory.

8. PERFORMING ORGANIZATION REPORT NUMBER. Enter all unique alphanumeric report numbers assigned by the performing organization, e.g. BRL-1234; AFWL-TR-85-4017-Vol-21-PT-2.

9. SPONSORING/MONITORING AGENCY NAME(S) AND ADDRESS(ES). Enter the name and address of the organization(s) financially responsible for and monitoring the work.

10. SPONSOR/MONITOR'S ACRONYM(S). Enter, if available, e.g. BRL, ARDEC, NADC.

11. SPONSOR/MONITOR'S REPORT NUMBER(S). Enter report number as assigned by the sponsoring/ monitoring agency, if available, e.g. BRL-TR-829; -215.

12. DISTRIBUTION/AVAILABILITY STATEMENT. Use agency-mandated availability statements to indicate the public availability or distribution limitations of the report. If additional limitations/ restrictions or special markings are indicated, follow agency authorization procedures, e.g. RD/FRD, PROPIN, ITAR, etc. Include copyright information.

13. SUPPLEMENTARY NOTES. Enter information not included elsewhere such as: prepared in cooperation with; translation of; report supersedes; old edition number, etc.

14. ABSTRACT. A brief (approximately 200 words) factual summary of the most significant information.

15. SUBJECT TERMS. Key words or phrases identifying major concepts in the report.

16. SECURITY CLASSIFICATION. Enter security classification in accordance with security classification regulations, e.g. U, C, S, etc. If this form contains classified information, stamp classification level on the top and bottom of this page.

17. LIMITATION OF ABSTRACT. This block must be completed to assign a distribution limitation to the abstract. Enter UU (Unclassified Unlimited) or SAR (Same as Report). An entry in this block is necessary if the abstract is to be limited.

Final Report:

COOPERATIVE AGREEMENT W911NF2120140

Epitaxial Growth and Characterization of Topological α-Sn and α-$Sn_{1-x}Ge_x$ Films

Christopher Palmstrom

University of California, Santa Barbara

December 21, 2022

ABSTRACT

α-Sn, the diamond structure allotrope of Sn, is a zero-gap semiconductor with band inversion. Theoretical predictions suggest that epitaxial tensile strain induces a transformation to a topological insulator phase, while epitaxial compressive strain induces a transformation to a Dirac semimetal phase [1,2]. Furthermore, when this Dirac semimetal phase is confined, it forms a quasi-3D topological insulator phase [3,4]. Currently only these latter two phases have been experimentally verified. In this project, the aim has been to obtain a better understanding of the effect of strain and film thickness on the α-Sn band structure. Compressively strained films are grown epitaxially by molecular beam epitaxy (MBE) directly on closely lattice matched InSb(001) substrates. The tensile strain is induced by alloying the α-Sn with isovalent Ge (α-$Sn_{1-x}Ge_x$), which has a smaller lattice parameter. Hence, this alloying decreases the bulk alloy lattice constant, resulting in a tensile strained film when grown epitaxially on InSb. Both of the topological insulator phases are predicted to have a large bandgap (at low thicknesses due to quantum confinement) and surface states with carriers having a high group velocity (low effective mass and high mobility). The α-Sn based system is also expected to have less alloy disorder and anti-site defect issues as compared to the prototypical chalcogenide topological insulator system, $(Bi,Sb)_2(Se,Te)_3$. In order to more precisely study the electronic structure of α-Sn and α- $Sn_{1-x}Ge_x$, high quality single crystal films are needed. Hence, the initial studies were to optimize both the InSb substrate surface preparation prior to growth and the conditions during growth. It was found that α-Sn growth on Sb-terminated InSb(001) surface decreased indium segregation and thus widened the growth window for α-Sn. This was verified both by angle resolved photoelectron spectroscopy (ARPES) and quantum oscillations in low temperature magnetotransport. These unalloyed α-Sn films provided answers to longstanding questions in the literature on the details of the electronic structure and provided a good baseline to compare to tensile strained α-$Sn_{1-x}Ge_x$ samples. Initial α-$Sn_{1-x}Ge_x$ (α-SnGe) alloy growths were performed and characterized via ARPES and scanning tunneling microscopy (STM) and spectroscopy (STS) without exposure to air. These preliminary results show good agreement with theoretical predictions, but further analysis is still necessary. The knowledge of the electronic bulk and surface state band structures of topologically non-trivial α-Sn and α-SnGe is essential for eventual spintronic and quantum computing applications.

TABLE OF CONTENTS

1. INTRODUCTION

The linearly dispersing topologically non-trivial surface states (Dirac fermions) that form on three dimensional (3D) topological insulators (TI) surfaces can have many applications in spintronics and quantum information systems [5,6]. Theoretical predictions and experiments have shown that α-Sn ($Fd\bar{3}m$, 1 bilayer (BL) ≈ 9.5×10^{14} atoms/cm^2, Fig 1b) goes through multiple topological phase transitions between zero gap semiconductor, two dimensional (2D) TI, 3D TI, 3D Dirac semimetal (DSM), 2D DSM, and trivial insulator as a function of biaxial strain, orientation, and film thickness generating much interest as a testbed for topological phase transitions [1,2,4,7–11]. Exact results vary by research group, measurement technique, and crystallographic orientation. As α-Sn is a single element, it does not suffer from off-stoichiometry, compositional uniformity, and other defects seen in the compound topological materials. This, along with the high band velocity (long mean free path) makes it very attractive for high-mobility Dirac fermion transport studies and spintronics. Indeed, it has already shown remarkable switching efficiencies at room temperature, comparable to the chalcogenide TI's [12,13]. Most α-Sn is studied either in the bulk or as a thin film compressively strained to a slightly lattice mismatched substrate. Bulk-like α-Sn is a zero-gap semiconductor with band inversion at the Γ point [14]. Biaxial compressive strain opens up a gap in the in-plane direction while causing band overlap in the out-of-plane direction. This band overlap takes the form of Dirac crossings, forming a 3D DSM [7].Of particular emphasis in the literature: compressively strained α-Sn confined to a thickness approximately less than (1/$\mathbf{k_{DP}}$)—where $\mathbf{k_{DP}}$ is the position of the DSM Dirac point in the bulk band structure—transitions to a quasi-3D TI [15,16]. In addition, tensile strain is predicted to form a true 3D TI phase (band gap in all directions, at all film thicknesses) [1,2]. These transitions are shown schematically in Fig 1a. While the compressively strained DSM phase and quasi-3D TI phase have been often studied, the agreement between different studies is lacking. Therefore, as part of this study, we sought to more closely study pure α-Sn so that we might precisely determine the specifics of the band structure before alloying with Ge.

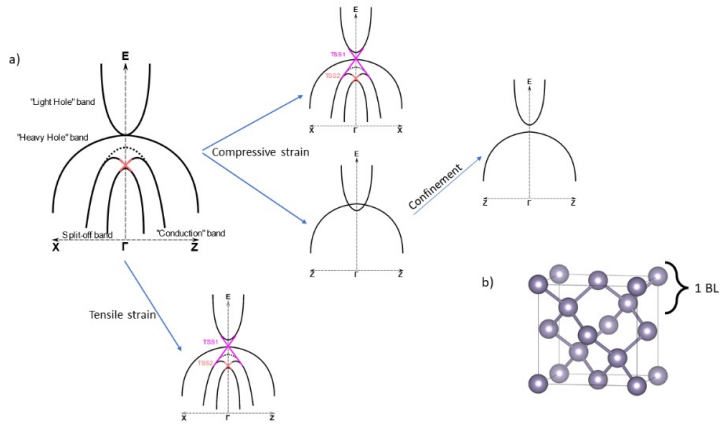

Figure 1 a) a schematic of the band structure changes of α-Sn. Biaxial compressive strain opens up a gap in plane and band crossings out of plane, forming a Dirac semimetal. Confinement by reducing film thickness gaps out the bulk Dirac crossings, forming a topological insulator. Alternatively, a topological insulator is formed by applying biaxial tensile strain. b) The diamond crystal structure of α-Sn, the layer corresponding to 1 bilayer (BL) is shown.

George de Coster at the Army Research Lab (ARL) has developed simulations which take into account film thickness, strain level, and film orientation. These simulations indicate that quantum confinement combined with tensile strain results in a large (≈300 meV) indirect bulk bandgap for 10-15 bilayers (BL, Fig. 1b) of Sn at 0.5% in plane tensile strain [17]. We aim to achieve this tensile strain by alloying α-Sn with isovalent Ge, shifting the bulk lattice constant to be smaller than that of the InSb substrate. In this case (10-15 BL), alloying Ge should preserve the quasi-3D

TI state while perhaps inducing slightly gapped surface states. In the thicker case (3D DSM), alloying Ge to apply tensile strain to the film should transition the DSM to a true 3D TI with a smaller bandgap (50 BL, 50 meV gap [17]).

Angle resolved photoelectron spectroscopy (ARPES) is an excellent technique for studying topology in materials as it directly measures the band structure and the existence of topological surface states [18,19]. Measuring the band structure via ARPES will readily elucidate changes in the Fermiology of our α-Sn and α-SnGe alloys to detect changes in the topology. To our knowledge, these will be the first α-SnGe thin films studied by ARPES. However, ARPES is a very surface sensitive and somewhat local measurement, which can sometimes obscure important features in the bulk band structure. Due to this surface sensitivity, ARPES must be performed on films with pristine surfaces that have not been exposed to the ambient. In our measurements, ARPES is performed via vacuum suitcase (base pressure $<5\times10^{-11}$ torr) transfer to synchrotron ARPES beamlines to preserve the surface cleanliness.

ARPES is a relatively local probe technique (beam radius approximately 100 μm), which in addition to the aforementioned surface sensitivity necessitates other characterization techniques to confirm the results. To supplement the ARPES measurements, bulk sensitive magnetotransport measurements were performed. Using Shubnikov-de Haas oscillations at low temperature, the carrier density and Berry phase of each band can be found from the frequency and phase, respectively, of the individual oscillation. The effective mass of each band can be found from the temperature dependence of the oscillations, the filling of each band by the oscillation frequency, and the 2D-ness of each band from the angular dependence of the oscillations. These results can then be directly compared to the ARPES measurements.

These measurements were further supplemented by *in-situ* reflection high energy electron diffraction (RHEED), and scanning tunneling microscopy (STM) and spectroscopy (STS), and *ex-situ* x-ray diffraction and in the near future with transmission electron microscopy (in-progress).

Furthermore, α-Sn is the low temperature stable allotrope of Sn. α-Sn transitions to a topologically trivial, metallic, superconducting, tetragonal phase (β-Sn) above 13.2 ºC. Fortunately, this phase transition temperature can be raised upwards of 100ºC by epitaxial stabilization via molecular beam epitaxy (MBE) growth of α-Sn (a=6.4892 Å) on closely lattice matched substrates like InSb (a=6.4794 Å) and CdTe (a=6.482 Å) [20]. While CdTe is a good substrate by lattice constant (and indeed has been used frequently for α-Sn growths in the past) the generally poor crystal quality with irremovable Te inclusions in the substrate create issues of reproducibility of the film growth. These Te inclusions may serve as nucleation sites for β-Sn [21]. Conducting CdTe substrates are also not readily available, complicating most surface science studies due to charging effects. Thus, the substrate used in this project has been conducting InSb.

We first optimized the growth of α-Sn on InSb(001), and then began growing α-SnGe on the same substrate. Although the epitaxial stabilization generally raises the α→β transition temperature from 13 °C to >100 °C [20], growth is still generally performed at temperatures at or below room temperature (RT) [22]. This is also done to reduce any segregation of In and Sb from the substrate into the Sn film. Indium serves as a *p*-type dopant while antimony serves as an *n*-type dopant [23]. The presence of large amounts of indium has also been found to harm the structural quality of the α-Sn film, likely through an antisurfactant-like mechanism [24]. ARPES is a filled state measurement, thus if the Fermi level is below the Dirac node of the surface states (roughly located near the bulk valence band maximum), changes to the node will be difficult measure. Since the

presence/absence of a gap in the surface states is a key parameter in topological phase transitions, it is essential that it is experimentally visible. In addition, many proposals to make use of topological insulators rely on transport of just the spin-polarized surface states. In this case, the chemical potential should be in the bulk bandgap to reduce the bulk carrier density. The "undoped" chemical potential is expected to be at the Dirac node (which is just above the valence band maximum, VBM). Thus, *p*-type doping due to indium segregation from the substrate should be avoided as much as possible, while *n*-type doping due to antimony segregation is, if anything, beneficial as it would raise the Fermi level. Indium segregation is typically limited by using a bismuth or tellurium surfactant layer deposited before Sn growth proceeds or by co-doping the Sn with tellurium during growth. Bi possibly obscures certain signatures of Sn due to its high spin-orbit coupling (SOC). Te may possibly have a similar issue, as Bi/Te samples have a higher measured surface state group velocity [22]. Te also forms very stable compounds with Sn, Sb, and In, leading to potential issues with impurity phases [25,26]. These dopant procedures are generally combined with the low temperature growths discussed above. Low temperature growth does, however, also appear to result in lower structural quality of the films [27]. Thus, none of these "solutions" are ideal. Adding a Ge effusion cell to begin growing α-$Sn_{1-x}Ge_x$ also effectively doubles the heat load on the sample due to the additional hot Ge effusion cell, making very cold substrate temperature growths more difficult.

After optimizing the growth temperature, growth rate and the InSb(001) substrate surface termination, we have successfully been able to grow high quality α-Sn directly without the addition of Te or Bi. This approach may allow higher growth temperatures of α-Sn and α-SnGe, without incorporating high concentrations of In. As discussed below, we have obtained some of the highest resolution ARPES measurements which confirm the topological insulator state of thin α-Sn. We possibly observe the topological surface state from the α-Sn/InSb interface. We then initiated alloying Ge into the Sn films to induce the tensile strain. Ge alloying was found to cause surface roughening, but high quality ARPES spectra are still observable. The initial ARPES and STS spectra agree with the prediction of a topological insulator state in tensile strained α-Sn.

2. OPTIMIZATION OF α-Sn GROWTH

2a. Growth Temperature

As α-Sn is the stable low temperature phase of Sn, control of temperature is critical to growing high quality films. It is possible that growing at higher temperatures could preferentially nucleate β-Sn over α-Sn. In addition, it has been reported that higher temperature growths led to severe segregation of In and Sb from the InSb substrate into the α-Sn thin film [22]. In the vertical VG-V80 MBE used for our growth, rotating the sample to face the liquid nitrogen cryopanel for cryocooling was not possible. Thermocouple measurements at these low temperatures are not accurate as it is not in physical contact with the sample. Two main "growth temperatures" were investigated through the course of our work 1) "room" temperature and 2) the "coldest" temperature. "Room" temperature was achieved by 1 W of radiative backside heating while being radiatively cooled by the cryopanel resulting in a substrate thermocouple reading of ~23 °C. The sample temperature is probably higher as liquid gallium (T_{melt} = 29.8°C) held at this temperature did not freeze. The "coldest" temperature consisted of a thermocouple reading between -15 and –23 °C depending on the thermal history of the chamber (i.e. first growth of the day or fifth growth of the day). This was achieved by no substrate heating, loading in the sample to the MBE chamber, and letting the sample radiatively cool for approximately 30 minutes. The cooling power was such

that liquid gallium starting at ~80 °C froze in under 10 minutes of this passive cooling. Growth at "room" temperature of 6 BL of α-Sn on an In-terminated InSb(001)-c(8x2) surface (not shown) resulted in the Sn surface morphology seen by others [22,28], with small "nuggets" dispersed throughout the sample. This could be evidence of In-Sn droplets,nucleation of β-Sn or strain induced by the Sn-dimer surface reconstruction.

2b. Growth Rate

α-Sn grows in a layer-by-layer fashion on InSb(001) [27,29]. This behavior was confirmed for our growths via reflection high-energy electron diffraction (RHEED) oscillations. However, the morphology of α-Sn is not as smooth as the RHEED oscillations might imply. The α-Sn(001) had a morphology, shown in Fig 2e and Fig 2f, of BL terraces decorated with a wormy structure. This morphology is typical for this substrate and orientation [11,22,28]. By looking at the distribution of heights in Fig 2f, we find that one "layer" of the grainy structure approximately corresponds to 1 BL of α-Sn. Further studies to confirm the relation between the wormy structure and the growth mechanism are in progress. At the "coldest" temperature layer-by-layer growth was found to be

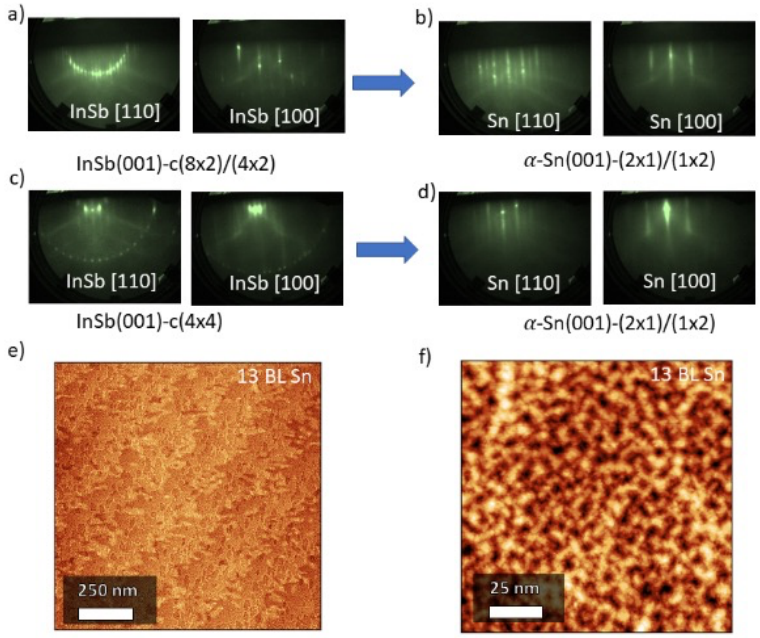

Figure 2 a), c) the RHEED pattern for the InSb-c(8x2) and InSb-c(4x4) reconstructions. b),d) the RHEED pattern for the mixed (2x1)/(1x2) reconstruction after 13 BL of Sn is deposited. No difference in pattern is evident. e) a 1000 nm x 1000 nm in-situ STM scan at 100 pA and 3 V f) a 100 nm x 100 nm scan under the same conditions

sustained for growth rates from 0.5 BL/min to 1.5 BL/min, but above 2 BL/min no oscillations in the RHEED intensity were observed. No clear dependence of oscillation amplitude and damping was found as a function of temperature, contrary to a prior report [27]. However, from an adatom mobility argument one would expect better layer-by-layer growth at higher temperatures (in the absence of dewetting).

2c. Effect of InSb Surface Termination on In and Sb Incorporation

After optimizing growth rate and growth temperature, we sought to investigate the influence of the surface termination of InSb(001) on the growth and properties of the α-Sn. In most prior studies of α-Sn growth, the Sn has been grown on the c(8x2) In-rich reconstruction of InSb(001) as seen in Fig 3a [30]. This is the usual surface reconstruction that forms after the sputter cleaning and annealing process that has typically been used to prepare a clean InSb(001) surface. A recent *in-situ* MBE growth of α-Sn/InSb also used this reconstruction [11]. As mentioned earlier, indium incorporation into the α-Sn films is often an issue with doping and may also lead to rougher surfaces [4,22,31]. Indium is a good *p*-type dopant in α-Sn resulting in the Fermi level being deep in the valence band below the Dirac point and bulk band gap [32].

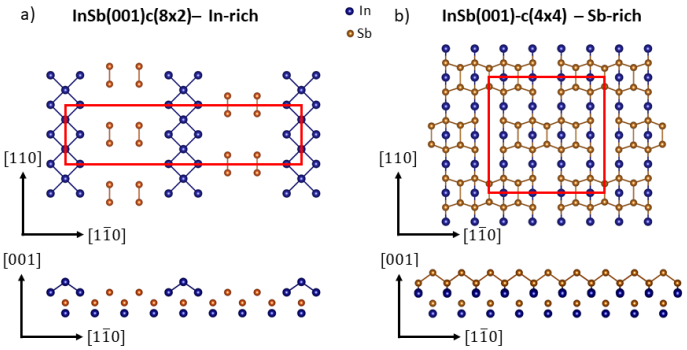

Figure 3 Two surface terminations of InSb(001), with surface unit cells framed in red. a) the In-rich c(8x2) reconstruction. b) the Sb-rich c(4x4) reconstruction [30]

In order to study the effects of Ge alloying on the topological insulator properties of α-Sn, it is essential to measure the behavior of the Dirac point—gapping out, for example. Additionally, to isolate the topological transport it is necessary to minimize the bulk carrier density by having the Fermi level in the bulk bandgap. Indium incorporation is normally limited in three ways. The first is growing as cold as possible [22]. The second is depositing an atomic layer of bismuth before proceeding with Sn growth [4]. The bismuth rides on the surface of the Sn film, promoting good growth as a surfactant. However, this makes attributing band structure changes difficult as Bi is a heavy metal and topological in its own right. In addition, the Bi could add non-trivial signals to eventual spin transport measurements on these films. The final method is using Te to both reduce (but not remove) the In segregation and also *n*-type dope the films to compensate the In *p*-type doping [3,31]. This method works, however SnTe and InTe have very high formation energies, and clusters of each could be forming in the film [25,26].

Our goal is to grow phase pure α-Sn without significant indium interdiffusion at growth temperatures greater than room temperature. The temperature is important as incorporating Ge requires an additional effusion cell for deposition. The additional heat load of this cell (operating at >1000 °C) could then increase the substrate temperature during α-SnGe growth. By performing growth on an Sb-rich InSb(001) surface reconstructions, such as the c(4x4) surface shown in Fig 3b [30], In incorporation is hoped to be kept at a minimum. This reconstruction involves a complete Sb- bulk terminated surface layer with an additional 0.75 ML Sb on top (1.75 ML total Sb at the surface) [30]. The Sb-termination should limit the amount of indium that is able to incorporate into the growing α-Sn film. In order to investigate this effect, two samples of two thicknesses (13 BL and 50 BL) were grown on two surface terminations. The oxide of the InSb(001) substrate was first removed by atomic hydrogen cleaning with a thermal cracker cell (MBE Komponenten). The samples were heated to 300 °C and exposed to the atomic hydrogen for 30 minutes at a chamber pressure of 5×10^{-5} Torr. This cleaning resulted in the In-rich c(8x2)/(4x2) InSb(001) surface reconstruction resulting in the RHEED diffraction patterns shown in Fig 2a. This surface cleaning procedure is expected to be much gentler than sputter cleaning

using an ion beam that most previous studies have used. The Sb-rich c(4x4) reconstruction was prepared by cleaning a sample in the same conditions and then annealing under an Sb_4 overpressure at around 50°C above the transition between the c(4x4) and a(1x3) reconstructions [33]. The corresponding RHEED diffraction patterns of the substrates prior to Sn deposition are depicted in Fig 2c. Care was taken to avoid Sb clusters on the surface by minimizing Sb exposure during the post-anneal cool down The InSb(001) surfaces were also characterized by *in-situ* STM, not shown. α-Sn was then grown on each sample at a rate of 0.5 BL/min at "room" temperature. In growth on both terminations, layer-by-layer growth proceeded with one layer corresponding to 1 BL. The RHEED patterns of 13 BL Sn is shown in Fig 2b and Fig 2d, both showing (2x1)/(1x2) Sn surface reconstruction. The surface morphology of Sn in both cases is approximately identical consisting of a wormy structure overlaid on the bilayer terrace structure (Fig 2e,f).

Using angle resolved photoemission (ARPES) to study the 13 BL films, the surface band structure is directly measurable. By using a photon energy of 21 eV, the spectra are very sensitive to the surface states. We concentrate on the surface states here as we can fit the linear Dirac cone and use the distance between the Dirac node (where the two linear bands intersect) and the Fermi level as a quantification parameter. As seen in Fig 4b,c, the Fermi level of α-Sn grown on the In-terminated InSb is approximately 100 meV below the Dirac node while growth on the Sb-terminated InSb has a chemical potential approximately at the Dirac node. Nominally this corresponds to a change in surface state density from ~4×10^{12} /cm^2 to 0 (accounting for the almost identical Rashba surface states [11]). However, this is not an accurate quantification of the reduction of In doping, as we are observing the surface projection of the bands (subject to band bending) rather than the dispersion in the bulk. [34]

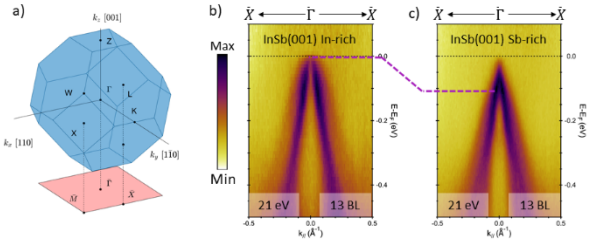

Figure 4 a) schematic of the bulk and surface (001) fcc-like Brillouin zones measured in ARPES. b) ARPES spectrum of the surface states of 13 BL Sn/In-terminated InSb(001), measured at 21 eV with p-polarized light. c) the same for 13 BL Sn/Sb-terminated InSb(001)

The indium reduction is confirmed by ultraviolet photoemission (UPS) shown in Fig 5. We find that indium incorporation in the films is reduced by several orders of magnitude. By switching between two different photon energies to modify the photoelectron inelastic mean free path (IMFP) (effectively probing depth of the measurement), we find that In has a higher concentration closer to the InSb interface. The indium reduction has a concomitant increase in the Sb incorporation. By increasing the gain on the UPS electron detector, we enhance the signal from indium (Fig 5c,d) and find that a small amount of indium is incorporated even for the Sb-terminated InSb.

We then change the photon energy to 127 eV and perform ARPES measurements on the bulk bands near the bulk Γ_{003} point (Fig 6a) as the photon energy is related to k_z by $k_z = \frac{1}{\hbar}\sqrt{2m_e(E_k cos^2(\theta) + V_0}$, where V_0 is the inner potential (a material-specific parameter describing the surface potential). An inner potential of 9.3 eV [11] was used as it was measured in a similar photon energy range used here, while the older reported value of 5.8 eV was measured using soft X-rays [10]. The expected bulk band structure (Fig 6b) is reflected in the measurements of Sn on both Sb-terminated (Fig 6c) and In-terminated (Fig 6d), the only change being the aforementioned 100 meV shift in chemical potential. This confirms that our substrate modification procedure is not measurably modifying the band structure of the α-Sn. The additional feature

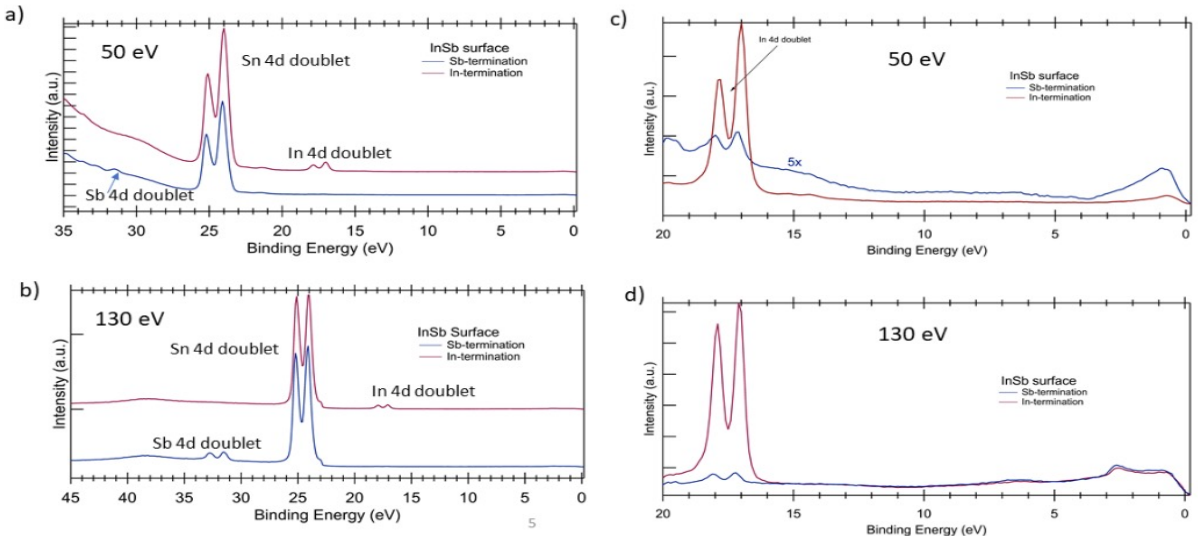

Figure 5 UPS measurements of 13 BL Sn films a) survey scan of Sn/In-terminated and Sb-terminated InSb with a photon energy of 50 eV, offset for clarity b) the same with a photon energy of 130 eV, offset for clarity c) and d) a zoom-in of a),b) on the In 4d states shows incomplete, but substantial, removal of In from the Sn films. The IMFP of Sb 4d states using 50 eV light is approximately double that using 130 eV photons (9.8 Å vs 5.4 Å)t. The IMFP of In 4d states using 130 eV light is approximately 20% greater than that using 50 eV light (5.7 Å vs 4.7 Å). The inelastic mean free path (IMFP) of Sn does not vary significantly. IMFPs are estimated via the universal curve.

shown approximately 200 meV below the Dirac node is possibly the surface state from the Sn/InSb interface, as suggested by our collaborators at ARL.

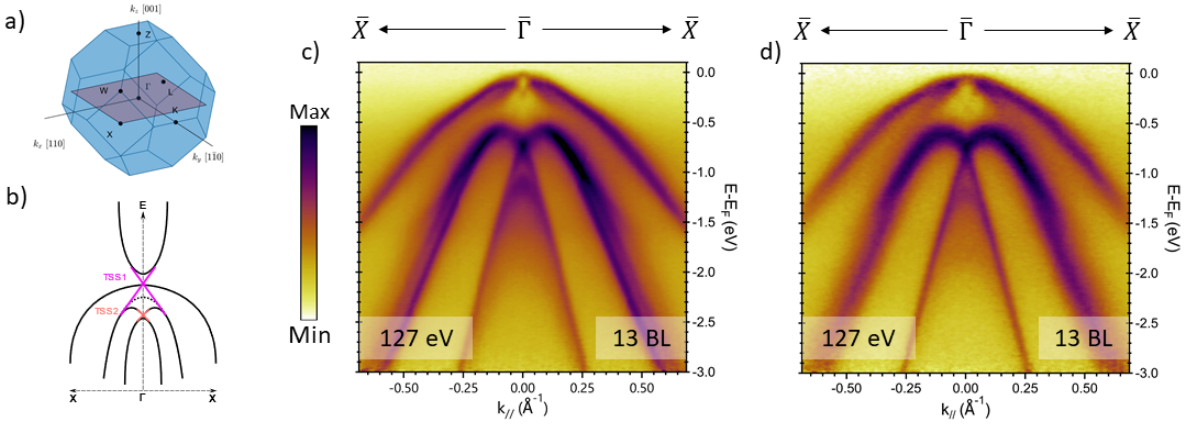

Figure 6 a) schematic of the slice of the bulk Brillouin zone taken during this measurement using a photon energy of 127 eV. b) The expected band structure of α-Sn. c) the bulk band structure of 13 BL of Sn grown on Sb-terminated InSb. d) the same but grown on In-terminated InSb.

While ARPES and UPS did confirm our method succeeded, those measurements are still very surface sensitive which is especially important when band bending is relevant. To confirm our results, magnetotransport measurements were performed in a van der Pauw geometry with silver paint contacts. Normal In solder and pulsed In soldering were investigated, but both seemed to significantly heat the Sn films, leading to potential β-Sn formation. The samples used for this study were 56 BL thick and without a capping layer so will have a native surface oxide. The thicker films were to 1) have a significant amount of film left over after oxidation (estimated consumption ~1-2 nm) and 2) dominate in the transport studies. InSb is a conducting substrate whose free carriers

do not fully freeze out at the temperature the measurements were performed (2 K). In future studies we will investigate $In_{1-x}Al_xSb$ buffer layers that have a larger bandgap than InSb that should result in reduced bulk parallel conduction. The longitudinal magnetoresistance for 50 BL Sn on In-terminated and Sb-terminated InSb (Fig 7a) shows a drastic difference between the two different substrates. A significant difference is also seen in the transverse resistance (Fig 7b) with the carriers changing sign and their density. The sharp increase in resistance at approximately 4 Tesla in both configurations is due to magnetic induced carrier freeze out of the InSb [34]. Clear Shubnikov-de Haas oscillations are visible for both samples. The oscillations were isolated by subtracting a polynomial fit to the background. After this, a fast Fourier transform (FFT) was performed to back out the frequency of each oscillation. Each frequency corresponds to the cross-sectional area of a certain band in the Fermi surface. This then corresponds to the carrier density associated with that band [35]. Two "matching" bands show up in both films as shown in Fig 7c. Each pair shows a reduction in frequency (and thus carrier density) confirming the above analysis via photoemission. In the Sb-terminated sample, an additional band at 50 T appears. This could be a higher harmonic or another band, further measurements are currently being performed to investigate. While the two bands that reduce in frequency are likely coming from the α-Sn, further confirmation is necessary. Data analysis is currently being performed to measure the effective mass of each band. Finally, angular dependence of the SdH oscillations in the geometry shown in Fig 7d was performed on the Sn/Sb-termination sample. As shown in Fig 7e, the 13 T band does not disperse as a function of angle. This band can then be called 2D-like and associated with the α-Sn surface states. Enhanced at higher angles, however, is a high frequency oscillation. This can also be seen in a slight peak at 100 T in Fig 7c. This oscillation, with a very high carrier density, is likely from the InSb substrate. [36]

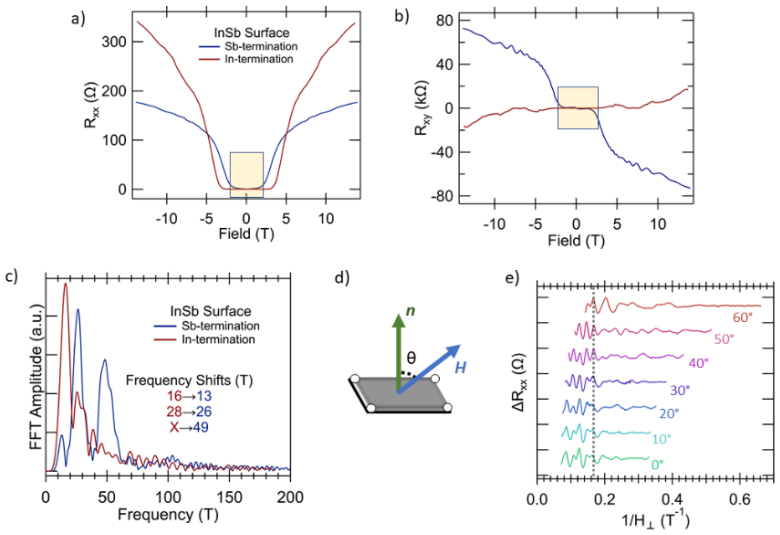

Figure 7 a) Longitudinal magnetoresistance curves for the two 56 BL samples. b) transverse magnetoresistance curves for the two 56 BL samples. Clear changes in carrier type and concentration are evident. The sharp change at approximately 4 T is explained in the text. c) the FFT of the background subtracted data in a). d) the schematic for the angular dependence measurement in e). e) angular dependence of oscillation frequency shows 2D or 3D structure. In this case, the 13 T band in c) is shown to be 2D like via a lack of angular dispersion.

2d. Confirming Topological Insulator State

After the initial predictions and confirmation of ultrathin compressively strained α-Sn being a topological insulator, there has been some disagreement in the literature between different groups and different measurement techniques [1,4,7,11,16,36]. One of the goals of our study was to find the wide bandgap TI state of α-SnGe under 0.5% tensile strain on InSb. However, we need to compare this to the "standard" 0.15% compressively α-Sn strained films on InSb(001). ARPES measurements have indicated that 13 BL of α-Sn to be a TI based on the presence of surface states

and comparison to DFT calculations [4,31]. A recent photoemission study found that the same surface states are present when α-Sn was compressively strained but not confined (the 3D DSM phase) at 370 BL [11]. From analysis of magnetotransport measurements it has been proposed that ultrathin (10-25 BL) α-Sn is a 2D Dirac semimetal instead of a quasi-3D TI [9]. In order to provide further clarification to these transitions, we used the earlier studied 13 BL Sn/Sb-terminated InSb(001). By dosing the surface with an alkali metal, in this case potassium, we induce downward band bending at the surface due to electron transfer from the potassium to the Sn, effectively raising the chemical potential at the surface observed via ARPES. By comparing the surface state measurements in Fig 8a,b, we find this shift to be approximately 200 meV. The Dirac node, which is clearly visible, does not appear directly gapped out (Fig. 8b). In addition, we see a second band nested in the electron-like Dirac cone. This is likely a 2DEG subband induced by the downward band bending at the surface. In Fig 8c, we again look at the bulk Γ point. We see no evidence of the conduction band. With the combination of ungapped topological surface states and a bulk band gap, we confirm that 13 BL α-Sn/InSb is a topological insulator. One caveat here is that the theorized bulk Dirac crossing is not actually at the bulk Γ point, but at a k_z= 0.039 Å^{-1}. However, in ARPES we do not truly slice the bulk Brillouin zone (in this case k_z=0) as a delta function, but rather as a Lorentzian whose full width to half maximum (FWHM) is the inverse of the approximate photoelectron escape depth [37], in this case approximately 0.1 Å^{-1} (compared to the Dirac node spacing of 0.078 Å^{-1}). Therefore, even though we are not measuring with a photon energy corresponding to the Dirac band crossing, the conduction band should still be visible in our spectra if it were present.

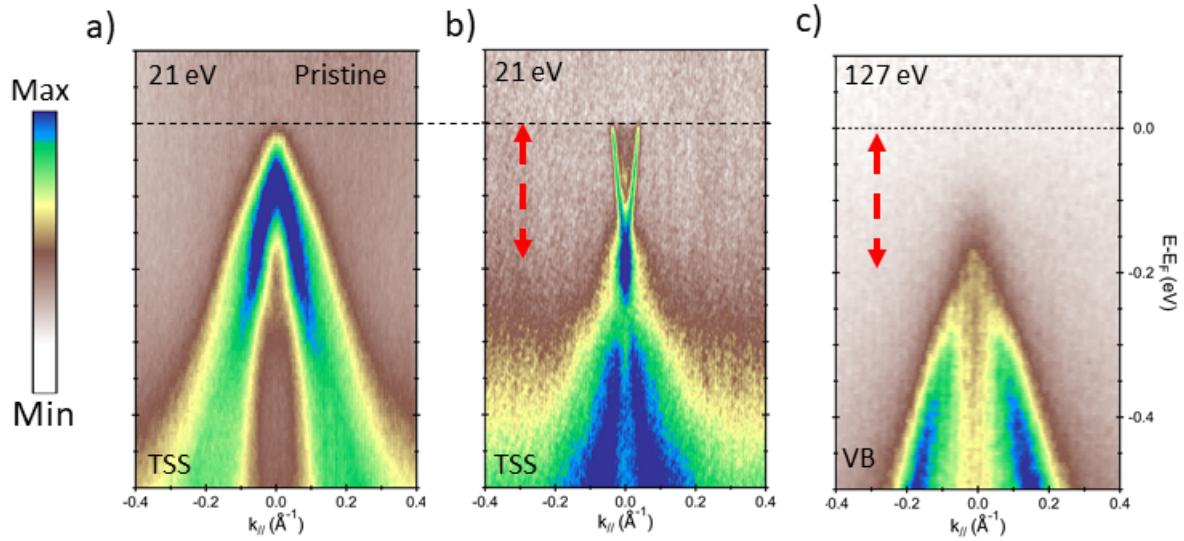

Figure 8 a) The topological surface state of 13 BL of Sn grown on Sb-terminated InSb. No gap is shown in the Dirac cone. b) K-dosing shifts the chemical potential up by approximately 200 meV. This causes the bottom Dirac cone to become gapped out. In addition, an additional band is nested in the electron-like Dirac cone. This is likely a 2DEG subband. c) The bulk bands are gapped out, no bulk conduction band is visible.

3. INITIAL STUDIES OF α-$Sn_{1-x}Ge_x$

3a. α-$Sn_{1-x}Ge_x$ Growth

After having optimized our ARPES scan conditions, substrate preparation, growth conditions, and fully established the 13 BL α-Sn reference, we started to alloy our films with Ge. We increased the growth rate of these films as the total radiative heat load is lessened by growing faster (time exposure outpaces increases in radiative heating from higher cell temperatures for our conditions). The Sn cell flux was held constant while varying Ge flux, thus the growth rate slightly changes for different Ge concentrations. The "coldest" temperature was used for growth to account for radiative Ge cell flux heating. Ge alloyed films continue to have the mixed (2x1)/(1x2) surface reconstruction in RHEED (Fig 9a,b) and growth still proceeds in a layer-by-layer manner as evidenced by RHEED intensity oscillations (Fig 9c). These oscillations supplemented Rutherford backscattering spectrometry measurements of films grown on Si to calibrate cell elemental fluxes. Alloying with Ge adds "nuggets" to the Sn morphology (Fig 9 d,e). This Ge concentration (15%) is above what is thought to be possible [38], potentially causing these nuggets by phase separation. The morphology remains generally the same in that we continue to have bilayer terracing with a wormy structure superimposed. However, the scale of the worminess is drastically different. This is first reflected in the both the RMS roughness and the average peak to valley distance increasing by approximately 50%. In addition, the kurtosis increases by a factor of two. On a closer comparison in Fig 9f,g, it is clear that the worminess is now thicker (increasing from +/- 0.7 nm to +/- 1.3 nm) and the individual worms are wider. This effect is likely from a combination of additional sample heating from the Ge effusion cell and the alloying of Ge itself. This morphology change is a function of Ge content (the worms are wider and deeper as Ge content increases).

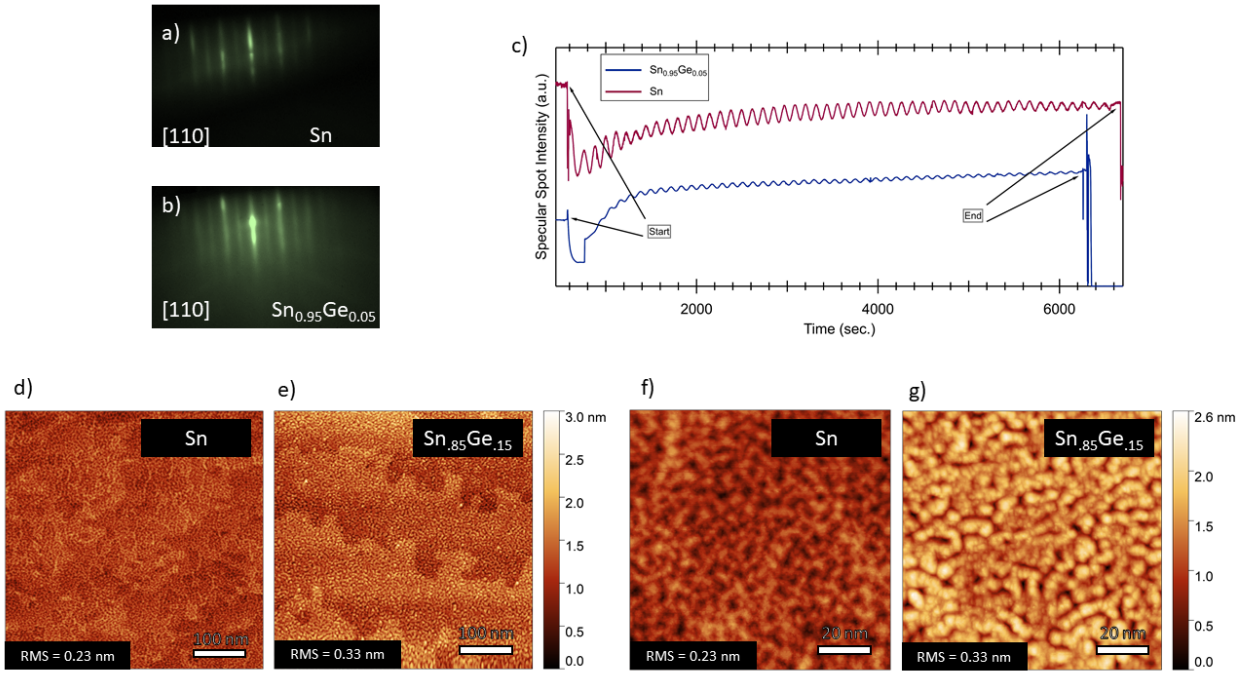

Figure 9 a) typical RHEED along the [110] for pristine Sn. b) typical RHEED along the [110] for α-SnGe. No change in reconstruction is seen. c) the RHEED intensity oscillates according to bilayer by bilayer growth for both α-Sn and α-SnGe. d), e) 500 nm x 500 nm in-situ¬ STM scans at 3 V and 100 pA for 13 BL α-Sn and 13 BL α-SnGe. f), g) 100 nm x 100 nm scans under the same conditions.

3b. α-SnGe Electronic Structure

We investigated two different paths on the α-SnGe electronic structure after discussing ideal conditions with our ARL collaborators. The first was to investigate the specific prediction of George de Coster at ARL of a wide bandgap TI when Sn is >0.5% tensile strain and confined to 10-15 BL. This was achieved by alloying Ge at 5% and 8% for 13 BL films. The dispersion of the surface states for pristine α-Sn is shown in Fig 10a. As mentioned in an earlier section, potassium-dosing reveals more information above the Dirac node in Fig 10b. However, the Dirac node is slightly gapped in 10b whereas it is ungapped in 10a. We initially thought this to be an artifact of alkali metal doping. However, upon Ge alloying we see this gap appears as well in Fig 10c,d. The cause of the gap then does not appear to be tensile strain, as the gap is formed in potassium-dosed compressively strained α-Sn. Nor does the gap appear to be a function of confinement, as the pristine α-Sn does not have a gap. Thus, the gap seems to be either a function of the Fermi level or the lattice distortion (separate from the epitaxial strain). This, and other explanations for this effect that are currently being investigated. Note that the shift in the Fermi level with respect to the Dirac node between 10a, c, and d could be from a changing band offset at either the vacuum/film interface, the film/substrate interface, or both. The band offset between Ge and InSb has not been measured to our knowledge. This argument is supported by the shift seeming to be a function of Ge content and depth. However, other explanations such as widening bandgap or increased Sb *n*-type doping are possible as well. In addition, very close to the Dirac node we observe a double peak. The peak is present in both Ge concentrations Fig 11a,b, but we do not have the resolution to observe it in the 13 BL Sn spectrum, if it exists. The double peak is clearer in the higher Ge content sample Fig 11d. By taking the curvature of the section, we enhance the contrast and see that the double peak appears to be two separate electron like bands that are degenerate away from the Γ point. This is possibly the Dirac surface states as the bottom band which then return to meet the bulk conduction band with a 30 meV gap between them. Further

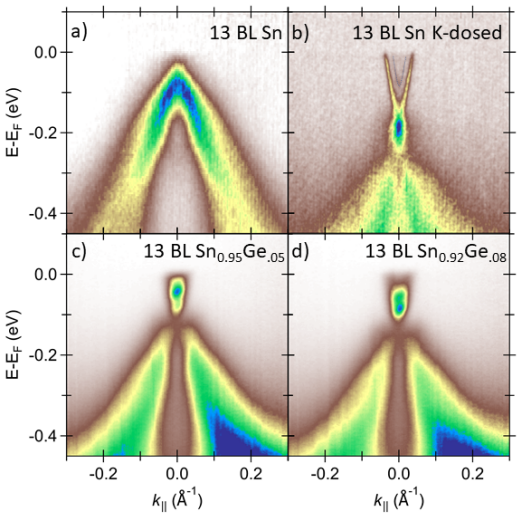

Figure 10 ARPES measurements at a photon energy of 21 eV measuring the surface states of a) pristine 13 BL Sn, b) K-dosing of the sample in a), c) 5% Ge alloying for the same sample thickness, d) 8% Ge alloying for the same sample thickness.

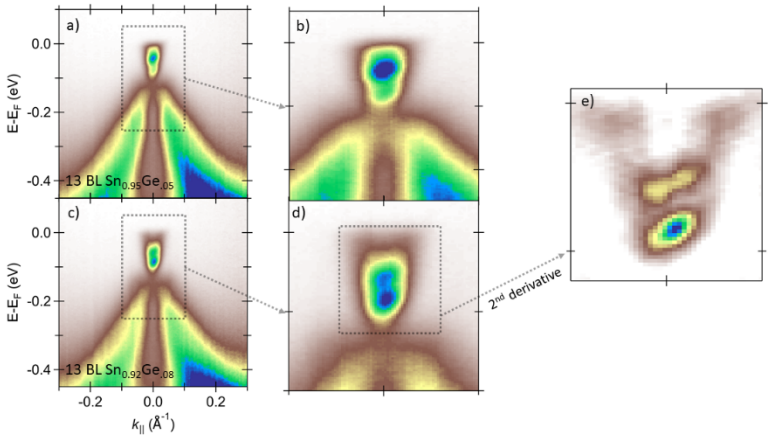

Figure 11 a) surface state measurement of 13 Bl 5% Ge SnGe. b) a close up showing slight gapping of the Dirac node. c) the same measurement as a) on 8% Ge SnGe. d) a close up showing the gapping, approximately the same size as b). e) Curvature enhances the dispersive features, showing two separate bands in place above the gapped surface states. Changes in chemical potential are likely from changes in band offsets.

measurements are necessary to confirm that this is the case. We have also taken bulk-sensitive spectra akin to Fig 6 that are still in the process of being analyzed.

The second path to investigate the electronic structure is to take α-Sn under compressive strain and no confinement (such that it is a Dirac semimetal) and replace the compressive strain with tensile strain. This strain is again achieved by alloying the α-Sn with Ge. There should be a topological phase transition between Dirac semimetal and topological insulator across this strain transition [1,2]. The surface states should then remain the same while the bulk gaps out. This effect was investigated in 50 BL of α-Sn, which should be firmly a DSM according to [9] and [4]. No noticeable change in the bulk band structure was observed (outside of a small rigid band shift, likely from the aforementioned band offsets). The surface state structure reflects this rigid band shift as well in Fig 12a, b with a slight change in the Fermi level. This is more evident in Fig 12c, where slices at a binding energy of 50 meV are compared. There is a clear contraction in the Ge alloyed case, associated with the chemical potential being closer to the node. In both samples, quantum well sub-bands are evident in the band structure, as are the Rashba surface states. The quantum well peaks are measured in Fig 12c, plotting the dashed line EDC slides at $0.1\pi/\mathbf{a}$. There appears to be a slight change in quantum well spacing, potentially from the change in effective mass between Ge alloyed α-Sn and pristine α-Sn. The absence of any intensity from the quantum well subbands at the Γ point precludes any attempts at quantification. The absence of intensity in this band is likely a matrix element effect observed in α-Sn before [10].

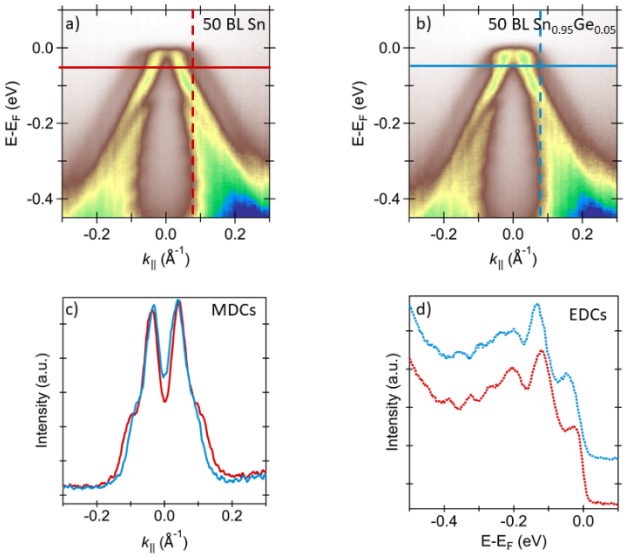

Figure 12 a) the surface states of 50 BL of Sn and b) SnGe. The Rashba surface states are evident in the broader brown background, as are quantum well states below 100 meV. c) Momentum distribution curves as depicted by solid lines in a) and b) at 50 meV binding energy a slight contraction of the peaks shows a slight change in chemical potential, again likely due to a change in VBO. d) the energy distribution curves drawn schematically by dashed lines in a) and b) at 0.1π/a. The quantum well subbands are evident. The spacing slightly changes, both from the rigid band shift and from Ge alloying.

Finally, we performed scanning tunneling microscopy and spectroscopy (STM/S) on the sample studied above at 77 K. The STS spectrum is approximately proportional to the DOS of the film. In Fig 13 we see the STM/S of the 50 BL Sn sample after synchrotron based ARPES measurements. Scanning tunneling spectroscopy measurements were performed at many different positions, as indicated in Figs. 13 and 14, to account for the "worms". We observe large changes to the DOS, likely as a function of effective α-Sn thickness, across these locations. Spectra at similar height

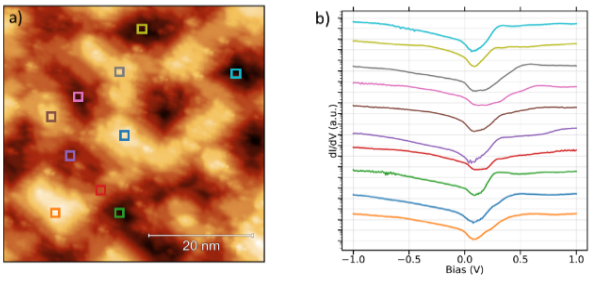

Figure 13 50 BL Sn after ARPES measurements a) 50 nm x 50 nm STM scan with STS taken at the locations highlighted b) STS spectra of the highlighted locations. There is no clear consistency across the measurements, but measurements at similar heights are similar

positions are similar. The only clear agreement across all measurements is the semimetallicity of the DOS, there is no true hard gap. The lack of hard gap is likely from the different surface states dispersing across the bulk band gap. When changing to the same thickness, but with Ge alloying (50 BL $Sn_{0.95}Ge_{0.05}$, Fig 14) there is now little consistency for DOS taken at similar height positions. This is likely an effect of the random alloy disorder of Ge on the (very local) DOS measurements, but more extensive analysis is needed. However, we do see that the distance between the VBM and the peak intensity of the DOS in the conduction band appears to increase with Ge doping. This suggests we have potentially widened the bulk bandgap by alloying Ge (inducing tensile strain), again a tentative agreement with predictions.

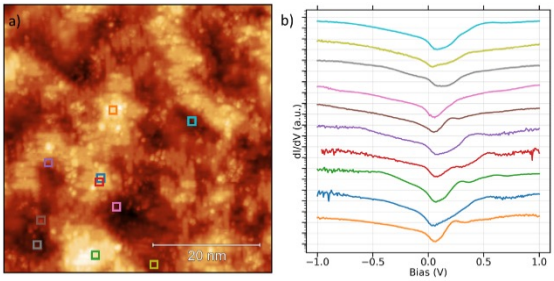

Figure 14 50 BL SnGe after ARPES measurements a) 50 nm x 50 nm STM scan with STS taken at the locations highlighted. B) STS spectra of the highlighted locations. There is not clear consistency among any of the measurements.

4. CONCLUSION

During the one year of the project, we accomplished much. First, we optimized our growths of α-Sn. We then charted a course for higher quality growths of α-Sn/InSb(001) in general by growing on Sb-terminated InSb(001). We cleared up confusion about the topological phase of ultrathin α-Sn and established a better baseline upon which to apply tensile strain with Ge alloying. In α-$Sn_{1-x}Ge_x$, we began to observe the effect of tensile strain on the unconfined and thickness confined α-Sn. We see clear shifts of Fermi level, likely from changes in band offsets. We find that the tensile strain does not appear to open a gap in the α-Sn surface states intrinsically, but the gap is actually a function of either band occupation or lattice distortion. We preliminarily confirm that α-$Sn_{1-x}Ge_x$ is a topological insulator in the ultrathin (15 BL) and thin (50 BL) cases.

5. FUTURE WORK

Outside of finishing the analysis on the data presented here, there are multiple paths to take. First and foremost is performing magnetotransport on the α-$Sn_{1-x}Ge_x$ films to confirm the surface sensitive ARPES measurements with SdH analysis. After these analyses, we would grow Sn and α-$Sn_{1-x}Ge_x$ on $In_{1-x}Al_xSb$. This serves as a barrier for back gating the samples to tune the sign and density of the free carriers. In addition, the VBO between Sn and InSb is likely different than that of Sn and AlSb. By changing the Al composition x, we could potentially tune the valence band offset (VBO) as well. These approaches could potentially help reduce the number of bulk carriers in the system. Spin polarized ARPES measurements will also be performed on both α-Sn and α-SnGe to confirm the topological nature of the surface states. Performing these measurements on a wider range of thicknesses and Ge concentrations would help elucidate the full form of the topological phase transition.

6. REFERENCES

[1] S. Küfner, M. Fitzner, and F. Bechstedt, *Topological α-Sn Surface States versus Film Thickness and Strain*, Phys Rev B **90**, 125312 (2014).

[2] H. Huang and F. Liu, *Tensile Strained Gray Tin: Dirac Semimetal for Observing Negative Magnetoresistance with Shubnikov-de Haas Oscillations*, Phys Rev B **95**, 201101 (2017).

[3] A. Barfuss, L. Dudy, M. R. Scholz, H. Roth, P. Höpfner, C. Blumenstein, G. Landolt, J. H. Dil, N. C. Plumb, M. Radovic, A. Bostwick, E. Rotenberg, A. Fleszar, G. Bihlmayer, D. Wortmann, G. Li, W. Hanke, R. Claessen, J. Schäfer, *Elemental Topological Insulator with Tunable Fermi Level: Strained α-Sn on InSb(001)*, Phys Rev Lett **111**, 157205 (2013).

[4] Y. Ohtsubo, P. le Fèvre, F. Bertran, and A. Taleb-Ibrahimi, *Dirac Cone with Helical Spin Polarization in Ultrathin-Sn(001) Films*, Phys Rev Lett **111**, 216401 (2013).

[5] M. Z. Hasan and C. L. Kane, *Colloquium: Topological Insulators*, Rev Mod Phys **82**, 3045 (2010).

[6] Y. Ando, *Topological Insulator Materials*, J Physical Soc Japan **82**, 102001 (2013).

[7] C. Z. Xu, Y. H. Chan, Y. Chen, P. Chen, X. Wang, C. Dejoie, M. H. Wong, J. A. Hlevyack, H. Ryu, H. Y. Kee, N. Tamura, M. Y. Chou, Z. Hussain, S. K. Mo, and T. C. Chiang, *Elemental Topological Dirac Semimetal: α -Sn on InSb(111)*, Phys Rev Lett **118**, 146402 (2017).

[8] C.-Z. Xu, Y.-H. Chan, P. Chen, X. Wang, D. Flötotto, J. A. Hlevyack, G. Bian, S.-K. Mo, M.-Y. Chou, and T.-C. Chiang, *Gapped Electronic Structure of Epitaxial Stanene on InSb(111)*, Phys Rev B **97**, 35122 (2018).

[9] L. D. Anh, K. Takase, T. Chiba, Y. Kota, K. Takiguchi, and M. Tanaka, *Elemental Topological Dirac Semimetal α-Sn with High Quantum Mobility*, Advanced Materials **33**, 2104645 (2021).

[10] V. A. Rogalev, T. Rauch, M. R. Scholz, F. Reis, L. Dudy, A. Fleszar, M.-A. Husanu, V. N. Strocov, J. Henk, I. Mertig, J. Schäfer, and R. Claessen, *Double Band Inversion in α-Sn: Appearance of Topological Surface States and the Role of Orbital Composition*, Phys Rev B **95**, 161117 (2017).

[11] K. H. M. Chen, K. Y. Lin, S. W. Lien, S. W. Huang, C. K. Cheng, H. Y. Lin, C. H. Hsu, T. R. Chang, C. M. Cheng, M. Hong, and J. Kwo, *Thickness-Dependent Topological Phase Transition and Rashba-like Preformed Topological Surface States of α-Sn(001) Thin Films on InSb(001)*, Phys Rev B **105**, 075109 (2022).

[12] J. Ding, C. Liu, V. Kalappattil, Y. Zhang, O. Mosendz, U. Erugu, R. Yu, J. Tian, A. DeMann, S. B. Field, X. Yang, H. Ding, J. Tang, B. Terris, A. Fert, H. Chen, and M. Wu, *Switching of a Magnet by Spin-Orbit Torque from a Topological Dirac Semimetal*, Advanced Materials **33**, 2005909 (2021).

[13] J.-C. Rojas-Sánchez, S. Oyarzún, Y. Fu, A. Marty, C. Vergnaud, S. Gambarelli, L. Vila, M. Jamet, Y. Ohtsubo, A. Taleb-Ibrahimi, P. le Fèvre, F. Bertran, N. Reyren, J.-M. George, and A. Fert, *Spin to Charge Conversion at Room Temperature by Spin Pumping into a New Type of Topological Insulator: α-Sn Films*, Phys Rev Lett **116**, 096602 (2016).

[14] S. Groves and W. Paul, *Band Structure of Gray Tin*, Phys Rev Lett **11**, 194 (1963).

[15] X. Xiao, S. A. Yang, Z. Liu, H. Li, and G. Zhou, *Anisotropic Quantum Confinement Effect and Electric Control of Surface States in Dirac Semimetal Nanostructures*, Sci Rep **5**, 7898 (2015).

[16] G. J. de Coster, P. A. Folkes, P. J. Taylor, and O. A. Vail, *Effects of Orientation and Strain on the Topological Characteristics of CdTe/ α -Sn Quantum Wells*, Phys Rev B **98**, 115153 (2018).

[17] G. J. de Coster, Personal communications.

[18] H. Zhang, T. Pincelli, C. Jozwiak, T. Kondo, R. Ernstorfer, T. Sato, and S. Zhou, *Angle-Resolved Photoemission Spectroscopy*, Nature Reviews Methods Primers **2**, 54 (2022).

[19] B. Lv, T. Qian, and H. Ding, *Angle-Resolved Photoemission Spectroscopy and Its Application to Topological Materials*, Nature Reviews Physics **1**, 609 (2019).

[20] R. F. C. Farrow, D. S. Robertson, G. M. Williams, A. G. Cullis, G. R. Jones, L. M. Young, and P. N. J. Dennis, *The Growth of Metastable, Heteroepitaxial Films of Alpha-Sn by Metal Beam Epitaxy*, J Cryst Growth **54**, 507 (1981).

[21] A. Kiefer, Personal communications.

[22] I. Madarevic, U. Thupakula, G. Lippertz, N. Claessens, P. C. Lin, H. Bana, S. Gonzalez, G. di Santo, L. Petaccia, M. N. Nair, L. M. C. Pereira, C. van Haesendonck, and M. J. van Bael, *Structural and Electronic Properties of the Pure and Stable Elemental 3D Topological Dirac Semimetal α-Sn*, APL Mater **8**, 031114 (2020).
[23] R. J. Wagner and A. W. Ewald, *Free Carrier Reflectivity of Gray Tin Single Crystals*, Journal of Physics and Chemistry of Solids **32**, 697 (1971).
[24] A. Giunto, T. Hagger, and A. F. i Morral, *Sn-In Co-Segregation and In Surfactant Effect in MBE in-Situ Doping of GeSn*, ArXiv (2022).
[25] M. Tang, D. W. Niles, I. Hernández-Calderón, and H. Hóchst, *Photoemission Study of the α-Sn/Cdte(110) Interface Growth*, MRS Online Proceedings Library (OPL) **94**, 213 (1987).
[26] H. Zimmermann, R. C. Keller, P. Meisen, and M. Seelmann-Eggebert, *Growth of Sn Thin Films on CdTe(111)*, Surf Sci **377–379**, 904 (1997).
[27] M. G. Betti, E. Magnano, M. Sancrotti, F. Borgatti, R. Felici, and C. Mariani, *Growth Morphology of (1x2) a-Sn(1 0 0): A Surface Diffraction Study*, Surf Sci **507–510**, 335 (2002).
[28] S. Kaku, K. L. Hiwatari, and J. Yoshino, *Scanning Tunneling Microscopy of Strained-α-Sn(0 0 1) Surface Grown on InSb(0 0 1) Substrate*, Appl Surf Sci **571**, 151347 (2022).
[29] P. Fantini, M. G. Betti, C. Mariani, E. Magnano, M. Pivetta, and M. Sancrotti, *The Pseudomorphic Growth of α-Sn on InSb(100): Electronic Structure and Morphological Properties*, Surf Sci **454–456**, 807 (2000).
[30] N. Jones, The Atomic Structure of of the Indium Antimonide (001) Surface, University of Leicester, 1998.
[31] M. R. Scholz, V. A. Rogalev, L. Dudy, F. Reis, F. Adler, J. Aulbach, L. J. Collins-Mcintyre, L. B. Duffy, H. F. Yang, Y. L. Chen, T. Hesjedal, Z. K. Liu, M. Hoesch, S. Muff, J. H. Dil, J. Schäfer, and R. Claessen, *Topological Surface State of $\alpha \textrm{-}{\rm Sn}$ on InSb(001) as Studied by Photoemission*, Phys Rev B **97**, 75101 (2018).
[32] I. Madarevic, U. Thupakula, G. Lippertz, N. Claessens, P. C. Lin, H. Bana, S. Gonzalez, G. di Santo, L. Petaccia, M. N. Nair, L. M. C. Pereira, C. van Haesendonck, and M. J. van Bael, *Structural and Electronic Properties of the Pure and Stable Elemental 3D Topological Dirac Semimetal α -Sn*, APL Mater **8**, 031114 (2020).
[33] W. K. Liu and M. B. Santos, *Surface Reconstructions of InSb(001) during Molecular Beam Epitaxy*, Surf Sci **319**, 172 (1994).
[34] S. Ishida, *Magnetic Freeze-out and Impurity Band Conduction in n-InSb*, Physica E Low Dimens Syst Nanostruct **18**, 294 (2003).
[35] D. Shoenberg, *Magnetic Oscillations in Metals* (Cambridge University Press, Cambridge, 1984).
[36] V. A. Rogalev, F. Reis, F. Adler, M. Bauernfeind, J. Erhardt, A. Kowalewski, M. R. Scholz, L. Dudy, L. B. Duffy, T. Hesjedal, M. Hoesch, G. Bihlmayer, J. Schäfer, and R. Claessen, *Tailoring the Topological Surface State in Ultrathin α -Sn(111) Films*, Phys Rev B **10**, 245144 (2019).
[37] V. N. Strocov, *Intrinsic Accuracy in 3-Dimensional Photoemission Band Mapping*, J Electron Spectros Relat Phenomena **130**, 65 (2003).
[38] R. A. Carrasco, S. Zollner, S. A. Chastang, J. Duan, G. J. Grzybowski, B. B. Claflin, and A. M. Kiefer, *Dielectric Function and Band Structure of Sn1−xGex (x < 0.06) Alloys on InSb*, Appl Phys Lett **114**, 062102 (2019).